Soft Matter

Cite this: *Soft Matter*, 2012, **8**, 2095

www.rsc.org/softmatter

PAPER

Ring polymers as model bacterial chromosomes: confinement, chain topology, single chain statistics, and how they interact

Youngkyun Jung,†*[a] Chanil Jeon,†[b] Juin Kim,†[b] Hawoong Jeong,[b] Suckjoon Jun[c] and Bae-Yeun Ha*[d]

Received 19th April 2011, Accepted 30th August 2011
DOI: 10.1039/c1sm05706e

Chromosomes in living cells are strongly confined but show a high level of spatial organization. Similarly, confined polymers display intriguing organizational and segregational properties. Here, we discuss how ring topology influences self-avoiding polymers confined in a cylindrical space, *i.e.* individual polymers as well as the way they interact. Our molecular dynamics simulations suggest that a ring polymer can be viewed as a "parallel connection" of two linear subchains, each trapped in a narrower imaginary tube. As a consequence, ring topology "stiffens" individual chains about fivefold and enhances their segregation appreciably, as if it induces extra linear ordering. Using a "renormalized" Flory approach, we show how ring topology influences individual chains in the long chain limit. Our polymer model quantitatively explains the long-standing observations of chromosome organization and segregation in *E. coli*.

I. Introduction

Living cells adopt various strategies to pack, organize, and partition their chromosomes, *i.e.* genetic materials that are highly packed inside the cell with their natural size a few orders of magnitude larger than the cell itself.[1,2] How they are organized or packed intramolecularly is not only crucial to such biological processes as transcription and replication but also has non-trivial impacts on their partitioning properties.[1–8] Of particular interest are the bacterial chromosomes, for which two competing views have recently been put forward concerning their segregation:[1,2,7–12] "assisted" and "spontaneous." The former focuses on protein-machinery, similar to mitotic spindles in eukaryotes that pull the sister chromatids apart during mitosis.[9,10] The other view, in contrast, emphasizes roles of the physical properties of the chromosome itself as a driving force for organization[2,5,11–13] and segregation.[2,7,11,12]

Along with the latter view, it is worth emphasizing that chain molecules such as DNA are distinct from a low-molecular weight liquid in the sense that their macroscopic behavior is largely insensitive to their molecular details (*e.g.* monomer shape), owing to chain connectivity.[14,15] This *universality* allows one to focus on their large-scale behavior independently of molecular details. A closely related point is that DNA-reshaping proteins (such as MukB and HU in bacteria[16,17] and histones in eukaryotes[18]) can be considered as modifying *locally* the physical properties of chromosomes; their effects have often been subsumed into "structural units" or effective monomers of the chromosome.[2,12,18,19] Along this line, it has recently been suggested that the role of these proteins is to create the right physical conditions for spontaneous segregation of chromosomes,[2] for example, by local compaction of each molecule, which enhances their segregation tendency.[12,20] These studies attest to the significance of interrelationships between the local action of proteins and large-scale physics.

Similarly, intramolecular organization of individual chromosomes in cells has also been studied.[3–5,13,21–24] For instance, the elastic filament model recently proposed[5] views the nucleoid as a homogeneous elastic medium. On the other hand, it is now widely known that cylindrical confinement induces linear ordering of a chain molecule, which would otherwise remain disordered[14] (also see ref. 2, 11, 25–28). Because of the long-recognized interplay between local chain packing and segregation tendency[20] (see ref. 2 and 12 for physical interpretations), it is desirable to present a model that captures this feature.

Indeed, there has been increasing effort to explore such models, in particular, polymer models of chromosomes.[2,11,12,18,24,29–32] The main conclusions from these models are: (i) (open) cylindrical confinement not only stiffens chain molecules but also enhances the tendency of chain segregation;[2,11,12] (ii) topological effects (ring or looping of the chains) can facilitate spontaneous segregation,[24,29–33] especially for the spherically confined case.

[a]*Supercomputing Center, Korea Institute of Science and Technology Information, Yuseong-gu, Daejeon, 305-806, Korea. E-mail: yjung@kisti.re.kr*
[b]*Department of Physics, Korea Advanced Institute of Science and Technology, Daejeon, 305-701, Korea*
[c]*FAS Center for Systems Biology, Harvard University, Cambridge, Massachusetts, 02138, USA*
[d]*Department of Physics and Astronomy, University of Waterloo, Waterloo, Ontario, Canada N2L 3G1. E-mail: byha@uwaterloo.ca*
† All of these authors made equal contributions.

In this article, we study how chain topology influences single chain properties and their mutual interactions under confinement, using molecular dynamics (MD) simulations and a scaling approach; each polymer chain consists of N monomers, trapped inside a cylindrical space of diameter D. Our simulations suggest that such a ring polymer can be viewed as a "parallel connection" of two linear subchains, each consisting of $N/2$ monomers trapped in a narrower "imaginary" tube.[34] As a consequence of this interrelationship, in an open cylindrical pore, ring topology "stiffens" individual chains about fivefold, as if linear ordering is much enhanced. Also we construct a "renormalized" Flory approach to ring polymers, similar to the previous one for a linear chain,[26] especially for calculating their elasticity and confinement free energy in the long-chain and large-D limit.

The imaginary-tube concept proves to be useful for understanding how ring topology enhances segregation tendency. Its effect is shown to be equivalent to trapping each subchain in a narrower tube, and as a result, ring polymers constrain and thus repel each other better than in the linear case. This is in contrast to the spherically-confined case, where linear chains intermingle, while ring polymers compartmentalize.[24,29–31]

Using polymer models (with ring topology), we show how *E. coli* chromosomes are intra- and inter-molecularly organized. In particular, we interpret the observations of linear ordering[4,5,21,22] and segregation[4,6,7] of the chromosomes (see also ref. 1 and 2 and those therein), and highlight the effects of ring topology.

This article is organized as follows. In section II, we outline the simulation procedure. In section III, simulation results are presented and the effects of chain topology are discussed, followed by a scaling analysis of chain confinement and topology. A polymer basis for both intra- and inter-chain organization of *E. coli* chromosomes is presented in section IV.

II. Molecular dynamics (MD) simulations

In our MD simulations, we use a bead-spring model of a (ring) polymer, trapped inside a cylindrical pore. Beads (among themselves and with the confining walls) interact *via* the fully-repulsive Weeks-Chandler-Andersen (WCA) potential,[35] given by

$$U_{\mathrm{WCA}}(r) = \begin{cases} 4\varepsilon\left[\left(\frac{\sigma}{r}\right)^{12} - \left(\frac{\sigma}{r}\right)^{6} + \frac{1}{4}\right] & \text{for } r < 2^{1/6}\sigma \\ 0 & \text{otherwise} \end{cases}, \quad (1)$$

where ε and σ represent the strength and range of the WCA potential, respectively. Finally, r denotes the center-to-center distance between two beads, or the distance of the bead center from the confining cylinder minus σ. As a result, the monomer size $a \approx \sigma$.

The bond between two neighboring beads is modeled by the finite extensible nonlinear elastic potential of the form

$$U_{\mathrm{FENE}}(r) = -\frac{1}{2}kr_0^2 \ln\left[1 - \left(\frac{r}{r_0}\right)^2\right], \quad (2)$$

where the molecular spring constant $k = 30\varepsilon/\sigma^2$ and the maximum bond length $r_0 = 1.5\sigma$.[36]

Newton's equations are integrated with the velocity Verlet algorithm with a time step $\delta t = 0.01\tau_0$, where $\tau_0 = \sigma\sqrt{m/\varepsilon}$ represents the characteristic time scale with bead mass $m = 1$. A Langevin thermostat is used to keep the system at the fixed temperature $T = 1.0\varepsilon/k_{\mathrm{B}}$, where k_{B} is the Boltzmann constant. The damping constant $0.1\tau_0^{-1}$ is used in all directions (see ref. 27 for details). Finally, we carry out 2000–10 000 independent simulations to obtain ensemble averages, *i.e.* averages over all the different simulations.

III. Results

A. Relaxation dynamics: chain topology

First, we have examined the time evolution of a ring polymer confined in an open cylindrical pore of diameter D, using two different initial conditions: (i) stretch-release and (ii) compression-release of the chain. For the former case, the chain is initially stretched much beyond its equilibrium conformation and then released. For the latter case, it is initially compressed by about 30% of its equilibrium size and then released. Here, we do not attempt to include hydrodynamic interactions (HI), but we concentrate on extracting information about chain elasticity. Thus the neglect of HI effects will not limit the applicability of our results. In principle, the earlier theoretical approach proposed in ref. 27 can be extended to examine HI effects.

Let $L(t)$ be the longitudinal size of a confined chain and L_0 its equilibrium value (see Fig. 1). For a linear chain, $L_0 \sim ND^{-2/3}$.[14] As evidenced later, this scaling behavior works for a ring polymer too. Clearly, $\langle L(t)\rangle \to L_0$ as $t \to \infty$, independently of the initial condition, where $\langle \ldots \rangle$ is an ensemble average. To study chain

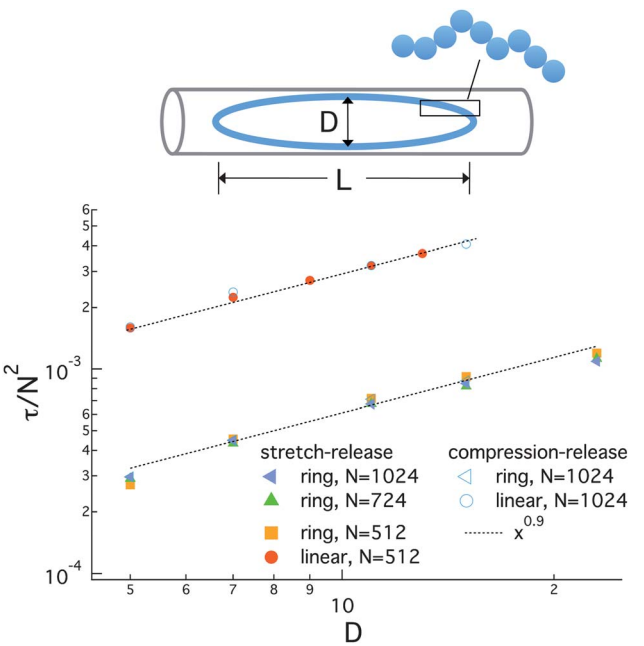

Fig. 1 Rescaled relaxation time, τ/N^2, as a function of D, obtained from stretch-release and compress-release simulations. For the same N and D, the ring polymer relaxes appreciably faster than the corresponding linear chain (see the legend) and is much "stiffer". (Error bars are smaller than the symbols used).

relaxation, we have examined the large-t behaviour of $\langle L^2(t)\rangle - \langle L(t)\rangle^2$, which is well approximated by a single-exponential decay, *i.e.* $\langle L^2(t)\rangle - \langle L(t)\rangle^2 \sim e^{-t/\tau}$, as in the case of linear chains.[27,28] The relaxation time τ can be obtained from the slope of a linear fit to large-t data for this quantity in a semi-log plot.[27]

Displayed in Fig. 1 are the resulting reduced relaxation times τ/N^2 of a ring polymer in a log-log plot as a function of the pore diameter D for a few choices of N (N = 512, 724, and 1024). Superimposed are our results for linear chains (N = 512 and 1024). The results in Fig. 1 show that $\tau \sim N^2D^{0.9}$ for both ring and linear chains. This finding confirms the recent numerical results for linear chains[26–28] but deviates from the earlier theoretical result (in the absence of HI effects), $\tau \sim N^2D^{1/3}$, based on the much-celebrated 'blob'-scaling approach.[25] The discrepancy has been extensively examined and attributed to finite chain-size effects.[26–28] The study in ref. 28 even suggests that the asymptotic scaling limit is hard to reach with the current computational power. In this connection, it is worth mentioning that the elastic response of an unconfined self-avoiding chain suffers from similar finite-size effects.[37] The force-extension relation based on the blob-scaling approach is predicted to be realized for $N \gtrsim 10^5$. Thus numerical and blob-scaling approaches need to be compared with caution.

Interestingly, the D exponent is the same for the ring and linear chains. The main difference between the two cases is through the x (= D) or y (= τ/N^2) intercepts. This implies that the difference can be taken into account by appropriately rescaling D and N, as detailed below, even though linear and ring polymers have different topology. This is a unique feature of cylindrical confinement and relies on the fact that individual chains and the way they interact can easily be modulated by changing D.

In order to study systematically the effects of chain topology on relaxation dynamics, we have explored a few strategies for mimicking ring topology and compared them in Fig. 2(a)–(c). In all cases, a ring polymer is considered as a parallel connection of two linear "subchains" (labelled in two different colors in Fig. 2), each consisting of $N/2$ monomers.

First, assume that the two subchains are "transparent" to each other, as illustrated by the cartoon on the left in Fig. 2. This picture is equivalent to using the rescaling $N \to N/2$ in τ/N^2 for the ring polymer. Fig. 2(a) shows the resulting relaxation time as a function of D. However, the data for the linear and ring chains do not collapse very well onto each other.

One way to include the subchain repulsion is to trap each subchain in an "imaginary tube" of reduced diameter, as illustrated in the cartoon on the right in Fig. 2. One plausible choice is $D/\sqrt{2}$, since this accounts for the reduced cross-sectional area each subchain chain occupies. When this imaginary-tube concept is introduced in Fig. 2(b) (in addition to the N rescaling in (a)), the agreement is somewhat better than in Fig. 2(a). As evidenced below, this strategy works well for large D.

Our last strategy is to use an effective diameter $D_{\rm eff}$ in our D rescaling by noting that monomers do not fill the cylinder uniformly in the direction normal to the symmetry axis of the cylinder. The effective diameter $D_{\rm eff}$ is defined as two times the weighted average of the normal distance from the symmetry axis r (not to be confused with r in section II) with respect to the monomer density $\rho(r)$. It can be obtained as $D_{\rm eff} = 2r_{\rho_{\max}}$ in the following relation: $\int_{r_{\rho_{\max}}}^{r_{\rm end}} \rho(r) r dr = \int_{r_{\rho_{\max}}}^{r_{\rm eff}} \rho_{\max} r dr$, where $\rho_{\max}$ is the maximum value of $\rho(r)$; $r_{\rho_{\max}}$ and $r_{\rm end}$ are the positions at $\rho(r) = \rho_{\max}$ and $\rho(r) = 0$, respectively. As it turns out, this is an excellent choice for collapsing the linear and ring cases, especially for small D.

Fig. 3 shows a linear relationship between $D_{\rm eff}$ and D for both ring and linear chains for $D \lesssim 10$: $D_{\rm eff} \approx 0.74D \equiv D_{\rm ring}$ for the ring chain and $D_{\rm eff} \approx 0.64D \equiv D_{\rm linear}$ for the linear chain. Because of the subchain repulsion, $D_{\rm eff}$ is somewhat larger for the ring polymer, as long as D is not too large. This indicates that the diameter is overcorrected in Fig. 2(b). According to our results in Fig. 3, the correct D rescaling is $D_{\rm linear} = \frac{1}{\sqrt{2}} D_{\rm ring}$. (Alternatively, we can rescale the diameter for the linear case as $D \to D\frac{1}{\sqrt{2}}\frac{D_{\rm ring}}{D_{\rm linear}} \approx D\frac{1}{\sqrt{2}}\frac{0.74}{0.64} \approx 0.82D$, while keeping the diameter for the ring case unchanged.)

Fig. 2(c) shows how the linear and ring cases map onto each other when this effective rescaling is used. The excellent agreement suggests that ring topology can be most accurately mimicked by the rescaling: $D_{\rm eff} \to \frac{1}{\sqrt{2}} D_{\rm eff}$ (together with $N \to \frac{1}{2}N$). Note this works for any D; for small D, $D_{\rm ring} > D_{\rm linear}$, but for large D, $D_{\rm ring} \approx D_{\rm linear}$. The effects of chain topology are also manifested in the effective spring constant $k_{\rm eff}$. Letting $k_{\rm linear}$ and $k_{\rm ring}$ be the effective spring constant of linear and ring polymers, respectively, our results in Fig. 2(c) and Fig. 3 suggest that for $D \lesssim 10$

$$\frac{k_{\rm ring}}{k_{\rm linear}} = 4\left(\frac{D_{\rm linear}}{D_{\rm ring}/\sqrt{2}}\right)^{0.9} \approx 4\left(\sqrt{2}\times\frac{0.64}{0.74}\right)^{0.9} \approx 4.81. \quad (3)$$

In other words, $k_{\rm ring} \approx 4.81 k_{\rm linear}$. As D increases, however, this relationship becomes less sensitive to the aforementioned feature of the ring polymer (thus $D \to \frac{1}{\sqrt{2}} D$ works) and is given by $k_{\rm ring} \approx 4(\sqrt{2})^{0.9} k_{\rm linear} \approx 5.46 \times k_{\rm linear}$.

B. Scaling approach to a ring polymer

Our simulation results suffer from finite-size effects.[26–28] Here, we construct an analytical approach to a ring polymer for $N \gg 1$ (or $N \to \infty$) and $D \gg a$. In this case, we expect $\rho(r)/\rho_{\max}$ to be similar for both linear and ring polymers. This means that a ring chain maps onto a parallel connection of two subchains, trapped in an imaginary tube of diameter $\frac{1}{\sqrt{2}} D$.

Recently, Jun *et al.*[26] proposed a renormalized Flory approach to a linear self-avoiding chain under cylindrical confinement, which correctly reproduces L_0 (the average chain size) and $k_{\rm eff}$ (the effective spring constant) predicted by the de Gennes' blob picture.[14,25] The confinement free energy of a linear chain as a function of the longitudinal chain size L is given by

$$\frac{\mathcal{F}_{\rm linear}(L)}{k_B T} = A\frac{L^2}{(N/g)D^2} + B\frac{D(N/g)^2}{L}, \quad (4)$$

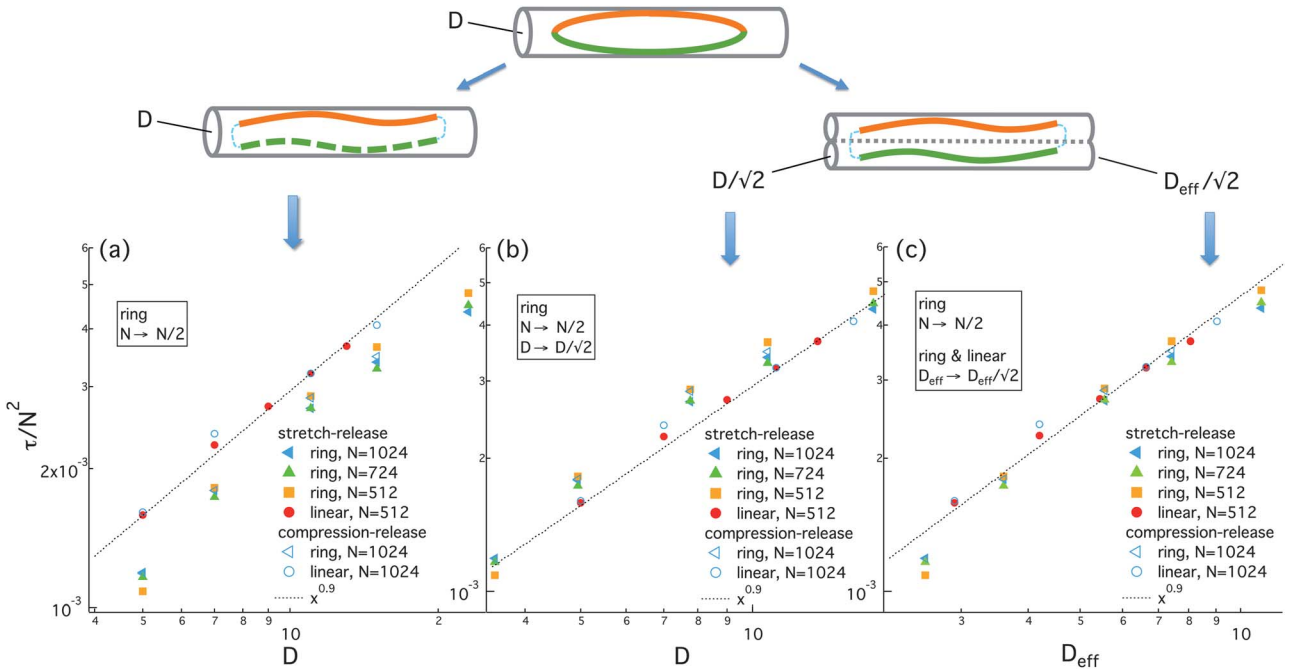

Fig. 2 Effects of ring topology and imaginary tubes: a few strategies for collapsing the data for linear and ring chains, thus mimicking ring topology. In all these cases, the ring polymer is considered as a parallel connection of two subchains labelled in two colors; this is equivalent to using $N \rightarrow N/2$ in τ/N^2 for the ring polymer. As indicated in the box, (a) $D \rightarrow D$, (b) $D \rightarrow D/\sqrt{2}$, and (c) $D_{\text{eff}} \rightarrow D_{\text{eff}}/\sqrt{2}$, where D_{eff} is the effective diameter (see the text for details). In (b) and (c), each subchain is assumed to occupy an imaginary tube of reduced diameters, $D/\sqrt{2}$ and $D_{\text{eff}}/\sqrt{2}$, respectively. The agreement between the linear and ring polymers is better in (c) than in (a) or (b) for the D range shown in the figure. Qualitatively speaking, the ring polymer makes better use of the confined space, exploring a larger cross-sectional area, than the corresponding linear chain, and each subchain occupies a tube of diameter somewhat larger than indicated in (b). For the asymptotic limit of $D \gg a$, however, the mapping in (b) is expected to work better.

where A and B are (non-universal) constants of the order of 1 and $g \approx D^{5/3}$ is the number of monomers per compression blob (*i.e.* an "imaginary sphere" beyond which self-avoidance is screened[14]). Here and below, lengths are estimated in units of a, unless otherwise stated. The free energy in eqn (4) leads to $L_0 = (B/2A)^{1/3} D(N/g) \approx (B/2A)^{1/3} N D^{-2/3} \equiv L_{\text{linear}}$. The confinement free energy at L_0 is $\mathcal{F}^0_{\text{linear}} = \left(3/2^{2/3}\right) B^{2/3} A^{1/3} (N/g)$ and $k_{\text{eff}} = \left(\frac{\partial^2}{\partial L^2} \mathcal{F}_{\text{linear}}\right)_{L_0} = 6AN^{-1}D^{-1/3} \equiv k_{\text{linear}}$ (in units of $k_B T$).[26,27] Note that this approach remains valid unless the chain is compressed too much longitudinally[26] (also see Fig. 5 and related discussions).

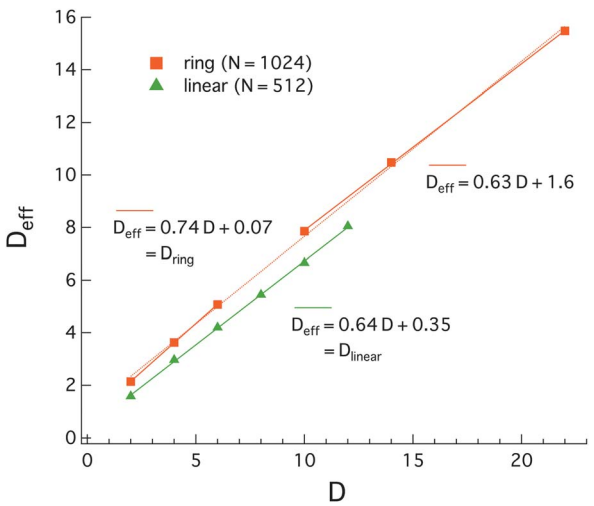

Fig. 3 The effective diameter D_{eff} for the linear and ring polymers. Crudely speaking, D_{eff} is two times the average of r weighted with respect to the monomer density $\rho(r)$, where r is the normal distance from the symmetry axis of the cylinder. Our results here show how D_{eff} deviates from the geometrical diameter D.

To extend our scaling approach to the case of a confined ring polymer, let parameters with a hat be the renormalized ones that correctly capture effects of ring topology. Then the confinement free energy can be written as

$$\frac{\mathcal{F}_{\text{ring}}(L)}{k_B T} = 2\left[A\frac{L^2}{(\hat{N}/\hat{g})\hat{D}^2} + B\frac{\hat{D}(\hat{N}/\hat{g})^2}{L}\right] \approx \hat{A}\frac{L^2}{(N/g)D^2} + \hat{B}\frac{D(N/g)^2}{L}, \quad (5)$$

where $\hat{A} = 2^{13/6}A$ and $\hat{B} = 2^{1/6}B$. Note here that the parameters g, N, and D in the second term on the right hand side are for the corresponding linear case. The equilibrium size, at which $\mathcal{F}$ is minimized, is given by $L_{\text{ring}} = (\hat{B}/2\hat{A})^{1/3} D(N/g) \approx 2^{-2/3}(B/2A)^{1/3} N D^{-2/3} \approx 0.63 L_{\text{linear}}$ (recall $L_{\text{linear}} = (B/2A)^{1/3} D(N/g)$). The confinement free energy at L_{ring} then reads $\mathcal{F}^0_{\text{ring}} = (3/2^{2/3})\hat{B}^{2/3}\hat{A}^{1/3}(N/g) \approx 2^{5/6} \times (3/2^{2/3}) B^{2/3} A^{1/3} (N/g) = 2^{5/6} \times \mathcal{F}^0_{\text{linear}}$ (in units of $k_B T$).[38] This means that ring topology

almost doubles the confinement free energy; trapping each subchain in a tube (see Fig. 2) requires extra free energy. Furthermore, $k_{\mathrm{ring}} = \left(\frac{\partial^2}{\partial L^2}\mathcal{F}_{\mathrm{ring}}\right)_{L_{\mathrm{ring}}} = 6\hat{A}g/ND^2 \approx 2^{13/6} \times 6Ag/ND^2 = 2^{13/6}k_{\mathrm{linear}}$ (in units of k_BT) or $k_{\mathrm{ring}}/k_{\mathrm{linear}} \approx 4.49$. This deviates some what from the earlier result obtained for finite N and D. The main source for this discrepancy is the sensitivity of k_{eff} (especially its D dependence) to finite-size effects.[26–28]

The free energy $\mathcal{F}_{\mathrm{ring}}$ implies that chain back-folding (over length scales $>D$) is costly. Accordingly, it supports the blob picture in which a linear chain under cylindrical confinement can be viewed as a linear string of blobs.[14] This picture also applies to each subchain of a ring. Linear ordering of these blobs is a natural consequence of a high free-energy penalty for back-folding (see section IV for its implications). It also has physical consequences on chain miscibility or the way two confined chains interact, as detailed below.

C. Chain miscibility under cylindrical confinement

Our results for single chains have implications for the spatial organization of two (linear or ring) chains in a cell-like, closed cylindrical space. First, imagine compressing two linear chains against each other with an external force f, as illustrated in Fig. 4. It is easy to see that for small f the chains remain segregated. This can be understood as follows: chain segments in an overlapping region can be considered as two parallel subchains, resembling a (costly) ring polymer. This means that mixing is disfavored for weak f. This picture will break down if the chains continue to be compressed. The energy cost for self back-folding in the homogeneous or segregated region becomes comparable to that for chain overlapping. This will enhance chain miscibility.[12]

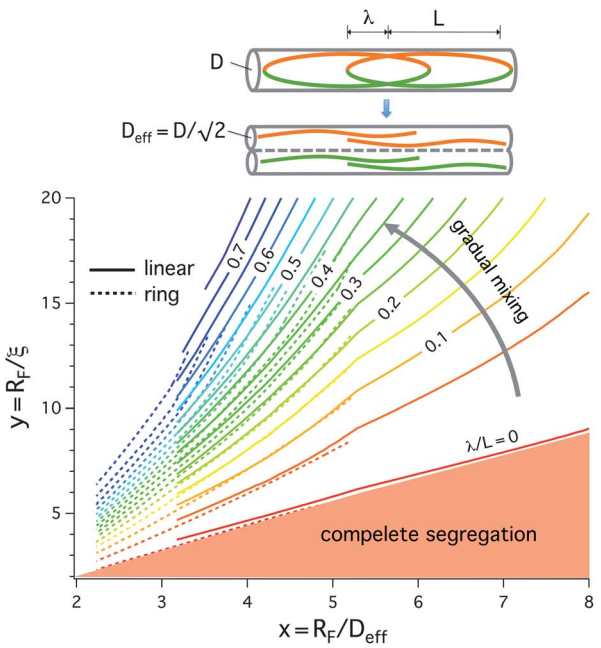

Fig. 4 Miscibility diagram displaying the fractional overlap distance, λ/L (= 0.1, 0.2, 0.3,…). The dotted lines describe ring polymers in a tube of effective diameter $D_{\mathrm{eff}}(= D/\sqrt{2})$, whereas the solid lines represent equivalent linear chains in a tube of diameter D. The two sets of diagrams collapse well onto each other. When chains are compressed, the reduced monomer density becomes more uniform (the chains are much compressed even for $\lambda/L \approx 0$). As a result, the mapping in Fig. 2(b) works well. Note that the two chains are practically segregated much beyond the shaded region (*e.g.* up to 50% of mixing). We predict that the *E. coli* chromosomes are in the spontaneous segregation regime.

It is gratifying that these arguments apply to the case of two compressed ring polymers. Ring topology in this case will change the energetics of overlapping and compression, but the qualitative picture of the linear case will remain applicable to the ring case.

We have plotted our simulation results for the fractional overlap distance λ/L in the diagram in Fig. 4 for both the ring (dotted lines) and linear (solid lines) cases; λ is the distance per chain between the two farthermost monomers belonging to different chains in the overlapping region. Here $R_F \sim N^{3/5}$ is the Flory radius or the chain size in an unconfined space and ξ is the blob size or the self-avoidance screening length.[14] Within each blob, self-avoidance dominates chain statistics; outside ξ, effects of the cylindrical wall and compression will be felt by the chain. In an open cylinder $\xi \approx D$. The diagram is based on our convention of $\xi = \phi^{-3/4}$, where ϕ is the volume fraction of monomers[14] and the numerical prefactor is set to unity.[39] Also, we choose $R_F = \text{const.} \times 1.11N^{3/5}$ in units of a, where the constant is introduced so as to account for the difference between linear and ring chains; const. = 1 for the former and 0.79 for the latter, which coincides with the ratio of the radii of gyration of the ring and linear chain. Finally, the numerical prefactor 1.11 is included to ensure the best fit to the simulation data.

Our diagram in Fig. 4 extends our previous work for linear chains[2,12] to the case of ring polymers. To understand the diagram, imagine crossing the miscibility diagram from left to right along a horizontal line. The fractional overlap distance λ/L decreases, *i.e.* the two chains become more segregable. This is equivalent to increasing the aspect ratio of the confining cylindrical box, while keeping the volume of the box fixed (thus the blob size ξ should remain constant).[40] Since the effect of ring topology is equivalent to reducing the diameter of the confining cylinder as explained in Fig. 2, ring polymers will always segregate better than linear chains.

In the shaded region below the bottom curve in red, chains remain completely segregated; note that on the curve, the chains are compressed against each other but resist mixing,[12] resembling touching 'cigars'.[41] Our diagram in Fig. 4 indicates that the boundary between the segregated and mixed regimes is a crossover for both linear and ring chains, not a sharp transition.[41] Chain miscibility is directly related to the degree of linear ordering each chain retains. As the two chains continue to be compressed against each other, each chain will lose linear ordering gradually. This explains the crossover behavior in our diagram in Fig. 4.

To collapse the two sets of diagrams, we have rescaled the diameter for the ring case as $D \to \frac{1}{\sqrt{2}}D$. Note this is consistent with the D rescaling used in Fig. 2(b), but the agreement is excellent. The additional factor discussed in Fig. 3 (*i.e.* $D_{\mathrm{ring}} \gtrsim D_{\mathrm{linear}}$) turns out to be insignificant when the chains are much compressed. In this case, $\rho(r)$ tends to a constant for both linear

and ring polymers, as our simulation data support (data not shown). As in the spherically confined case or in a unconfined space,[11] we find that ring topology enhances the segregation tendency under cylindrical confinement, as if it enhances linear ordering of the chain.

IV. Implications for bacterial chromosomes

To understand the physical properties of bacterial chromosomes and their functions, we need a simple, quantitative model that makes experimentally testable predictions. As a specific example, here we focus on the circular *E. coli* chromosome. Our view is that the *E. coli* chromosome is a "string of structural units", strongly confined in a closed space.[2,11–13,42] This is based on the following molecular and biological details: (i) Physical properties of the chromosome are determined not only by DNA strands but also by various proteins that interact with the DNA (see ref. 2, 17 and 43). (ii) When measured by fluorescence correlation spectroscopy,[44] an isolated *E. coli* chromosome appears to consist of "structural units." Each structural unit contains supercoiled plectonemes.[45] Physically, they are topologically constrained and should repel one another. (iii) Even inside the cell, the polymeric nature of bacterial chromosomes is well preserved, as evidenced in the subdiffusive dynamics of bacterial chromosomal loci.[46] In other words, chain connectivity plays an important role in chromosome relaxation in the viscoelastic cytoplasm.

Below we use the beads-on-string model of a chromosome, where each bead represents a structural unit. With this simplification, we can interpret recent experimental observations. Note that similar coarse-grained models have been used in the literature[11,12,18,42] (also see the endnote[19]).

A. Intramolecular organization of *E. coli* chromosomes

There have been a number of studies of the organization and dynamics of *in vivo* bacterial chromosomes using fluorescence imaging.[4,5,21,22] Some of the key observations relevant to us include: (i) a single chromosome before the onset of DNA replication is linearly ordered along the long axis of the cell (with a stretch of segments connecting the two poles of the packed chromosome),[4,5,21,22] and (ii) the distribution of the interloci distance follows the linear relation $\sigma_\Delta^2 \sim \Delta L \ll L_{\rm cell}$, where σ_Δ^2 is the variance of the interloci distance, ΔL, and $L_{\rm cell}$ is the cell length.[5]

Linear ordering of a chain molecule in a cylindrical space is now well understood.[2,11,13] We can also understand this by considering the free energy cost for chain back-folding under cylindrical confinement, as discussed in section III. Linear ordering of a ring polymer can also be understood similarly if we divide the ring into two linear subchains, as illustrated in Fig. 5, where we show a typical chain conformation from our simulations. The beads are colored progressively according to the color bar in the middle. We have chosen the parameters to mimic the *E. coli* chromosome (see subsection B for details): the number of structural units $n_{\rm d} = 200$, the diameter $D = 4.8$, and the cell or cylinder length $L = 28$ (in units of structural units). For these choices, $L_0 \approx 41$. (a) For a ring polymer (the upper figure), only one subchain is colored, with the other one in varying grey scale. Even under longitudinal compression as in *E. coli*, linear ordering of the subchain is well preserved. (b) The lower figures shows a single, linear subchain constructed with the same rescaling used for Fig. 4 or Fig. 2(b), *i.e.* $D \to D/\sqrt{2}$. This implies that our rescaling approach works even for the case of a compressed chain in an *E. coli* cell-like geometry.

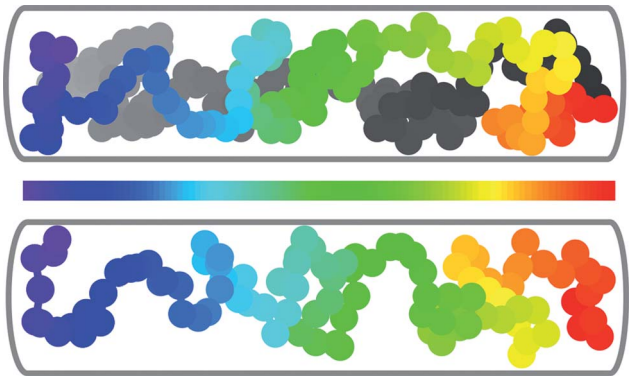

Fig. 5 Ring topology and linear ordering of a polymer in a closed bacterial cell-like geometry of length L and diameter D. A snap shot of a typical chain conformation is shown. The beads are colored progressively according to the color bar in the middle. We have chosen the parameters to mimic the *E. coli* chromosome. For a ring polymer (the upper figure), only one subchain is colored, with the other in a varying grey scale. A linear subchain constructed with the same rescaling used for Fig. 4, *i.e.* $D \to D/\sqrt{2}$ (the lower figure). We exaggerated the cylinder diameter in this case so that it matches with that in the ring case. Because of the D rescaling, the degree of linear ordering is comparable in the two cases.

The second observation $\sigma_\Delta^2 \sim \Delta L \ll L_{\rm cell}$ is also closely related to the linear ordering of the chromosome. To see this, note that the effective spring constant of a ring polymer under cylindrical pore is given by $k_{\rm eff} \sim 1/N \sim 1/L$.[26,28] Thus, as long as the linear ordering is preserved, $\sigma_\Delta^2 \sim 1/k_{\rm eff} \sim \Delta N \sim \Delta L$ as measured by Wiggins *et al.*[5] Furthermore, a recent study indicates $\sigma_\Delta^2 \ll L$ for a strongly confined chain,[28] a natural consequence of chain stiffening due to confinement. Although the scaling relationship for σ_Δ^2 can be understood straightforwardly, its proportionality constant has to be measured experimentally, since it will depend on many unknown (biological) details. Nevertheless, it is important to realize that the scaling relationship of the experimental data can be described by our simple polymer model.

B. Miscibility diagram and *E. coli*

Using the miscibility diagram in Fig. 4, we can quantitatively address the extent to which the ring topology of *E. coli* chromosomes will enhance their segregation tendency by revisiting the recent analysis in ref. 2 and 12. To this end, we summarize the measured parameters for *E. coli* and its chromosomes as follows. First, the *E. coli* chromosome consists of about 4.6×10^6 base pairs (bp), confined inside an overall-cylindrical space called the nucleoid,[45] with diameter $D \approx 0.24$ μm and length $L \approx 1.39$ μm[2,45,47] (see Fig. 1 in ref. 45 as well as the relevant point in ref. 48). Second, the size of the structural unit has been estimated by Krichevsky *et al.* to be $d \approx 70 \pm 20$ nm.[44] Third, recall $R_{\rm F} = {\rm const.} \times 1.11 d n_d^{3/5}$, where n_d is the total number of structural units of the chromosome and const. = 1 for a linear chain and

0.79 for a ring. Finally, the number of base pairs/domain is in the range of $g \sim 10\text{–}100 \times 10^3$ bp.[2,49] Thus, for 4.6×10^6 bp for the chromosome, n_d can be as small as 92 for $g = 50 \times 10^3$ bp[44] and as large as 230 for $g = 20 \times 10^3$ bp.[49] For the latter choice, it is natural to choose $d \approx 50$ nm, which is the lower bound for d and approximately corresponds to a close pack of such domains.

If we adopt $d = 70$ nm and $g = 50 \times 10^3$ bp (close to the upper bound of 100×10^3 bp) from ref. 44, we obtain $x \approx 6.88$ and $y \approx 17.37$,[48] corresponding to about 20% overlap for the linear chain case but $\approx 10\%$ for the ring polymer case. If we choose $g = 100 \times 10^3$ bp instead (for a more densely packed DNA in the chromosome), we obtain $\approx 10\%$ overlap for the linear chain case but much reduced $\approx 2\%$ for the ring polymer case. This analysis illustrates not only the significance of ring topology but also the interplay between packing and segregation: the chromosomes segregate better when more tightly packed, consistent with experiments.[20] Note that the two chains are practically segregated much beyond the shaded region (*e.g.* up to 50% of mixing) in the diagram in Fig. 4. Our analysis shows that the *E. coli* chromosomes are in the spontaneous segregation regime.

Our analysis provides a quantitative basis for the scaling picture of some aspects of topology-enhanced segregation (see Fig. 4 in Supplementary Information of ref. 2), which indicates enhanced segregation due to chain topology.

V. Conclusions

In this work, we have established an interplay between chain topology and confinement. Our results suggest that a ring polymer consisting of N monomers in a cylindrical pore of diameter D can be viewed as a "parallel connection" of two linear chains, each bearing $N/2$ monomers in an imaginary tube with a reduced diameter $\left(\approx \frac{1}{\sqrt{2}} D \text{ for } D/a \gg 1\right)$. As a result, ring topology "stiffens" a confined chain about fivefold, as demonstrated in Fig. 2.

Furthermore, this interrelationship is also manifested in the miscibility diagram in Fig. 4, which compares the effects of chain topology and confinement on chain miscibility. Adding ring topology to a linear chain is equivalent to reducing the diameter D to $D_{\text{eff}} = \frac{1}{\sqrt{2}} D$. In other words, a topological repulsion under cylindrical confinement can be translated into an equivalent confinement-induced repulsion.

Also the picture of such a confined chain as a linear array of blobs[14,25] is consistent with the recent observation of a linearly ordered *E. coli* chromosome in the nucleoid.[5] In our rescaling approach, the free energy penalty for chain back-folding (beyond the blob size) is similar to the extra confinement free energy caused by ring topology. It thus offers polymer (more microscopic) insights into linear ordering of chromosomes in rod-shaped bacteria (*e.g. E. coli*).[5] A closely related point is the picture of confined polymers as effective "repellers"—more so if more ordered. It thus supports the "internal" or spontaneous mechanism of chromosome segregation,[2,6,7,11,12] which relies on the physical properties of chromosomes themselves.

Despite molecular details being left out in our study, it is clear that the physical effects arising from confinement and chain topology play non-trivial roles in shaping individual chromosomes and their segregation, especially in elongated bacterial cells. Here, a direct experimental test of our model will be important for understanding the physical nature of the chromosome.

Acknowledgements

B.-Y.H. acknowledges the financial support of NSERC (Canada) and is grateful to C. L. Woldringh for stimulating discussions. This work was partially supported by APCTP (Y.J.) and by the Basic Science Research Program (2009-008769) through the NRF of Korea funded by the MEST (H.J.) as well as by Harvard University, USA, and the US National Institutes of Health (grant P50 GM068763 to S.J.). Helpful discussions with W. Wong and J. Pelletier are also acknowledged.

References

1 K. Bloom and A. Joglekar, *Nature*, 2010, **463**, 446–456.
2 S. Jun and A. Wright, *Nat. Rev. Microbiol.*, 2010, **8**, 600–607.
3 M. Thanbichler, P. H. Viollier and L. Shapiro, *Curr. Opin. Genet. Dev.*, 2005, **15**, 153–162.
4 H. J. Nielsen, Y. Li, B. Youngren, F. G. Hansen and S. Austin, *Mol. Microbiol.*, 2006, **61**, 383–393.
5 P. A. Wiggins, K. C. Cheveralls, J. S. Martin, R. Lintner and J. Kondev, *Proc. Natl. Acad. Sci. U. S. A.*, 2010, **107**, 4991–4995.
6 N. Kleckner, D. Zickler, G. H. Jones, J. Dekker, R. Padmore, J. Henle and J. Hutchinson, *Proc. Natl. Acad. Sci. U. S. A.*, 2004, **101**, 12592–12597.
7 M. C. Joshia, A. Bourniquel, J. Fisher, B. T. Hob, D. Magnana, N. Kleckner and David Bates, *Proc. Natl. Acad. Sci. U. S. A.*, 2011, **108**, 2765–2770.
8 C. L. Woldringh and N. Nanninga, *J. Struct. Biol.*, 2006, **156**, 273–283.
9 J. L. Ptacin, S. F. Lee, E. C. Garner, E. Toro, M. Eckart, L. R. Comolli, W. E. Moerner and L. Shapiro, *Nat. Cell Biol.*, 2010, **12**, 791–798.
10 E. Toro and L. Shapiro, *Cold Spring Harbor Perspect. Biol.*, 2010, **2**, a000349.
11 S. Jun and B. Mulder, *Proc. Natl. Acad. Sci. U. S. A.*, 2006, **103**, 12388–12393.
12 Y. Jung and B.-Y. Ha, *Phys. Rev. E: Stat., Nonlinear, Soft Matter Phys.*, 2010, **82**, 051926.
13 M. Buenemann and P. Lenz, *PLoS One*, 2010, **5**, e13806.
14 P.-G. de Gennes, *Scaling Concepts in Polymer Physics*, Cornell University Press, Ithaca, NY, 1979.
15 M. Doi and S. F. Edwards, *The Theory of Polymer Dynamics*, Oxford University Press, New York, 1988.
16 Z. M. Petrushenko, C.-H. Lai, R. Rai and V. V. Rybenkov, *J. Biol. Chem.*, 2006, **281**, 4606–4615.
17 J. Stavans and A. Oppenheim, *Phys. Biol.*, 2006, **3**, R1–R10.
18 J. F. Marko and E. D. Siggia, *Mol. Biol. Cell*, 1997, **8**, 2217–2231.
19 For an alternative view of DNA-bound proteins in *E. coli*, see ref. 2, where they are considered as increasing the correlation length of chromosomes, ξ_{chrom}, which is set to the size of "structural units" (also see section IV). It is not entirely clear how ξ_{chrom} and the blob size ξ defined in section III are related. Nevertheless, in both the view based on ξ_{chrom} and ours, DNA-organizing proteins act as segregation-enhancing agents (see section IV and ref. 12).
20 J. A. Sawitzke and S. Austin, *Proc. Natl. Acad. Sci. U. S. A.*, 2000, **97**, 1671–1676.
21 H. J. Nielsen, J. R. Ottensen, B. Youngren, S. J. Austin and F. G. Hansen, *Mol. Microbiol.*, 2006, **62**, 331–338.
22 X. Wang, X. Liu, C. Possoz and D. J. Sherratt, *Genes Dev.*, 2006, **20**, 1727–1731.
23 P. H. Viollier, M. Thanbichler, P. T. McGrath, L. West, M. Meewan, H. H. McAdams and Lucy Shapiro, *Proc. Natl. Acad. Sci. U. S. A.*, 2004, **101**, 9257–9262.
24 P. R. Cook and D. Marenduzzo, *J. Cell Biol.*, 2009, **186**, 825–834.
25 F. Brochard and P. G. de Gennes, *J. Chem. Phys.*, 1977, **67**, 52–56.

26 S. Jun, D. Thirumalai and B.-Y. Ha, *Phys. Rev. Lett.*, 2008, **101**, 138101.
27 Y. Jung, S. Jun and B.-Y. Ha, *Phys. Rev. E: Stat., Nonlinear, Soft Matter Phys.*, 2009, **79**, 061912.
28 A. Arnold, B. Bozorgui, D. Frenkel, B.-Y. Ha and S. Jun, *J. Chem. Phys.*, 2007, **127**, 164903.
29 J. Dorier and A. Stasiak, *Nucleic Acids Res.*, 2009, **37**, 6316.
30 S. Jun, A. Arnold and B.-Y. Ha, *Phys. Rev. Lett.*, 2007, **98**, 128303.
31 D. Marenduzzo and E. Orlandini, *J. Stat. Mech.: Theory Exp.*, 2009, L09002.
32 M. Bohn and D. W. Heermann, *PLoS One*, 2011, **6**, e14428.
33 T. Vettorel, A. Y. Grosberg and K. Kremer, *Phys. Biol.*, 2009, **6**, 025013.
34 The notion of a tube employed for a ring polymer here seems analogous to the one adopted in a different context, *i.e.* the 'reptational' motion of a linear polymer in concentrated solutions or melts.[14,15] However, there is also a difference: the tube in the former case takes into account "self constraint" within the same chain and thus works for cylindrical confinement only, while the tube in the latter captures effects of other chains. See the Results section for details.
35 J. D. Weeks, D. Chandler and H. C. Andersen, *J. Chem. Phys.*, 1971, **54**, 5237–5247.
36 K. Kremer and G. S. Grest, *J. Chem. Phys.*, 1990, **92**, 5057–5086.
37 G. Morrison, C. Hyeon, N. M. Toan, B.-Y. Ha and D. Thirumalai, *Macromolecules*, 2007, **40**, 7343–7353.
38 While the confinement free energy of a ring polymer can be obtained from our renormalized Flory approach in eqn (5), it is also derivable from that of the corresponding linear chain, which scales as $\beta\mathcal{F}_{\text{linear}} \sim ND^{-5/3}$. Then we find $\mathcal{F}_{\text{ring}}$ by rescaling D as $D \to \frac{1}{\sqrt{2}}D$: $\mathcal{F}_{\text{ring}} \approx 2^{5/6}\mathcal{F}_{\text{linear}}$, which is consistent with the analysis in the main text.
39 This relation, originally obtained for a semidilute polymer solution,[14] is based on the physical picture that a strongly-confined polymer is viewed as a "stack" of blobs[30]—inside each the chain resembles a self-avoiding walk. This picture works well for $\xi \gg a$ in the sense that the distinction between length scales $>\xi$ and $<\xi$ is not arbitrary. For $\xi \gtrsim a$, however, this relation can still be used as a measure of the degree of confinement, *i.e.* ξ defined this way can be considered as a length equivalent of ϕ. Within the scaling picture, the prefactor for the ξ-ϕ relation is not derivable. Note here that it suffices to use ξ consistently, *i.e.* with the same prefactor. Miscibility will not depend on the choice of the prefactor. Using a different prefactor will shift uniformly the contours in the diagram, but this is also reflected in the calculated $y = R_F/\xi$ value for a chain, so that this artifact will be cancelled out. Here, the prefactor is set to unity.
40 Along the line of this reasoning, one can argue that chain miscibility is also influenced by confinement even when chains are in the concentrated regime, where self avoidance is screened at all length scales ($\gtrsim a$) and linear chains mix. When trapped in a pore, especially as $D \to a$, however, the chains repel like "hard rods".[41] Our general picture of cylindrical confinement as inducing linear ordering and segregation works in the concentrated regime. (For a similar issue in a polymer melt, see J. L. Jacobsen, *Phys. Rev. E*, 2010, **82**, 051802. Also see ref. 33 for ring polymers in a melt).
41 M. Daoud and P. G. de Gennes, *J. Phys. Paris*, 1977, **38**, 85–93.
42 J. Fan, K. Tuncay and P. J. Ortoleva, *Comput. Biol. Chem.*, 2007, **31**, 257–264.
43 D. Skoko, D. Yoo, H. Bai, B. Schnurr, J. Yan, S. M. McLeod, J. F. Marko and R. C. Johnson, *J. Mol. Biol.*, 2006, **364**, 777–798.
44 T. Romantsov, I. Fishov and O. Krichevsky, *Biophys. J.*, 2007, **92**, 2875–2884.
45 See C. L. Woldringhand T. Odijk in *Organization of the Prokaryotic Genome*, edited by R. L. Charlebois (ASM Press, Washington, D.C. 1999).
46 S. C. Weber, A. J. Spakowitz and J. A. Theriot, *Phys. Rev. Lett.*, 2010, **104**, 238102.
47 S. Jun, http://arxiv.org/pdf/0808.2646v2?, 2009.
48 The values of L and D used in our miscibility calculations (Fig. 4) are, respectively, $L - d$ and $D - d$.[12] Also note that the values of L and D vary from reference to reference. Here we use those from ref. 47.
49 L. Postow, C. D. Hardy, J. Arsuaga and N. R. Cozzarelli, *Genes Dev.*, 2004, **18**, 1766–1779.

